energies

MDPI

Article

Optimal Design of Permanent Magnet Linear Generator and Its Application in a Wave Energy Conversion System

Hong-wei Fang [1,*], Ru-nan Song [1] and Zhao-xia Xiao [2]

1 School of Electrical and Information Engineering, Tianjin University, Tianjin 300072, China; songrunan@tju.edu.cn
2 Tianjin Key Laboratory of Advanced Electrical Engineering and Energy Technology, Tianjin Polytechnic University, Tianjin 300387, China; xiaozhaoxia@tjpu.edu.cn
* Correspondence: hongwei_fang@tju.edu.cn; Tel.: +86-138-2103-3642

Received: 9 October 2018; Accepted: 7 November 2018; Published: 10 November 2018

check for updates

Abstract: The emerging global wave energy industry has great potential to contribute to the world's energy needs. However, one of the key challenges in designing a wave energy converter (WEC) is the wave energy generator. Thus, this paper focuses on the optimal design of a cylindrical permanent magnet linear generator (CPMLG), which is used for the wave energy conversion system. To reduce the end effect and enhance the magnetic field performance of the CPMLG, the level-set method is applied to the design of the topology and size for the generator. In the paper, the objective air gap magnetic field is given by the mathematical analysis method and appropriate measuring points are predetermined. The measuring points can fully reflect the distribution characteristics of the air gap magnetic field. Then, topology evolution on the permanent magnet (PM) and yoke based on the level-set method are performed. The level set function corresponding to the initial shape of the PM is constructed. The algorithm is programmed and computed iteratively using the discrete time and space variables. Finally, the performances of the CPMLG with the updated PM and width of yoke are analyzed by ANSYS Maxwell. Results show that the magnetic field distortion and the unbalance of three-phase electromotive force (EMF) of the CPMLG is reduced by the optimization of the level-set method. It has also been verified that the designed CPMLG with the level-set method could be used for WEC at different wave conditions.

Keywords: magnetic field; level-set method; shape design; voltage unbalance; wave energy conversion

1. Introduction

Wave energy is an emerging renewable energy source, which can contribute towards sustainable development of our world [1–5]. Various wave energy generators have been used to convert wave power into useful mechanical power efficiently. The generator is one of the most important units in wave power generation system, so the design of the generator is crucial to the system efficiency. The ocean's environment is undetermined and unstable. To achieve relatively high quality and efficiency for converting ocean wave energy into electrical energy, various ocean wave energy converters and corresponding electrical machines have been investigated. It was found that linear generators can be used in the direct drive wave energy conversion system, in which it can reduce the complexity of mechanical transmission and improve the reliability and efficiency of the system [6–11]. Several electrical generator topologies have been analyzed in the past years [12,13]. When compared with the induction generator, doubly-fed induction generator, synchronous generator, and permanent magnet synchronous generator, the permanent magnet linear generator used in wave energy conversion seems to have a higher reliability and efficiency because the driving force of the linear motor is in a straight-line reciprocating direction [14,15]. In addition, the primary core of the permanent magnet linear generator can be sealed by epoxy resin and other materials after being embedded, which can be applied in the marine environment. However, due to the inherent edge effect and cogging effect of the permanent magnet linear motor, the resulting positioning force will cause the electromagnetic force of the motor to fluctuate, generate noise and resonance, and hinder the stroke of the secondary motion. At the same time, the fluctuation of the positioning force will cause the air gap magnetic field to be distorted, affecting the back electromotive force waveform, and reducing the power generation quality. Therefore, it is necessary to reduce the positioning force as much as possible with the level-set method, and this is also the key target for the design of permanent magnet linear generators, which are used for wave energy conversion [16].

The study of the level-set method can be traced back to the last century. In 1987, Sethian applied the upwind numerical solution scheme to the calculation of the interface evolution problem for the first time in the study of wave propagation, and gave the definition of the weak solution of the interface motion [17], which laid a theoretical foundation for the level set method. The following year, Osher and Sethian proposed the level set method, and gave the high-precision stable numerical solution of the level set equation [18]. At that time, this method was mainly used to solve the problem of flame shape change under the thermodynamic equation. Because of the highly dynamic change of the flame shape, the change of its topological structure with time is highly complicated, so it is difficult to describe the motion process accurately with the traditional parametric equation. Therefore, the level set method based on the time and motion interface arose at the historic moment [19]. After many years of development, the level-set method has been successfully applied in many fields, such as physics, fluid mechanics, materials science, and computer graphics. The level-set method and shape design sensitivity has been used for the rotor topology optimization of switched reluctance motor (SRM) in [20], in which the shape of the salient pole rotor determines the characteristic of the reluctance torque. Various torque ripples of permanent magnet (PM) machines are reduced by using different level set methods [21,22]. In this paper, to improve the air-gap magnetic field performance and reduce the unbalance of back-EMF, the CPMLG used for a wave energy conversion system is designed by using the level-set method to increase the wave energy capturing efficiency. Additionally, its validity has been verified by its application for direct and in-direct driving wave energy conversion systems, respectively.

2. Level-Set Method

2.1. Principle of Level-Set Method

Level-set methods (LSM) are a conceptual framework for using level sets as a tool for numerical analysis of surfaces and shapes. The advantage of the level-set model used in the optimization of the electrical machine is that it can perform numerical computations involving curves and surfaces on a fixed Cartesian grid without having to parameterize these objects. If the solution of the new level-set function evolution equation is presented and the position of each point for shapes of the electrical machine on the zero level set are deduced, then the result of the evolution curve or surface is obtained.

Suppose $\phi(x, y) = 0$ is the implicit level set function. Then, according to the principle level-set method, we can get the partial difference equation as:

$$\frac{\partial \phi}{\partial t} + \nabla \phi \cdot \frac{\partial C}{\partial t} = 0, \tag{1}$$

where $\nabla \phi$ is the gradient of ϕ, and $\frac{\partial C}{\partial t}$ represents the velocity field of the interface.

The curve, $C(t)$, obtained at pseudo time, t, is the solution of the zero level set, $\phi(C\,(x, y), t)$.

If the arc length of the curve is expressed by s, then according to the curve evolution theorem, it can be found that the change of ϕ along the tangential direction of C is 0, i.e., it exists.

$$\frac{\partial\phi}{\partial s} = \frac{\partial\phi}{\partial x}\cdot\frac{\partial x}{\partial s} + \frac{\partial\phi}{\partial y}\cdot\frac{\partial y}{\partial s} = \left\langle \nabla\phi, \frac{\partial C}{\partial s} \right\rangle = 0 \tag{2}$$

From Equation (2), it can be found that: $\nabla\phi \perp \frac{\partial C}{\partial s}$.
So, the normal vector of C can be represented as:

$$\vec{N} = -\frac{\nabla\phi}{|\nabla\phi|} \tag{3}$$

Thus, the level set evolution equation can be obtained as:

$$\frac{\partial\phi}{\partial t} = F|\nabla\phi| \tag{4}$$

The above level set evolution can be used for shape optimization as shown in Figure 1.

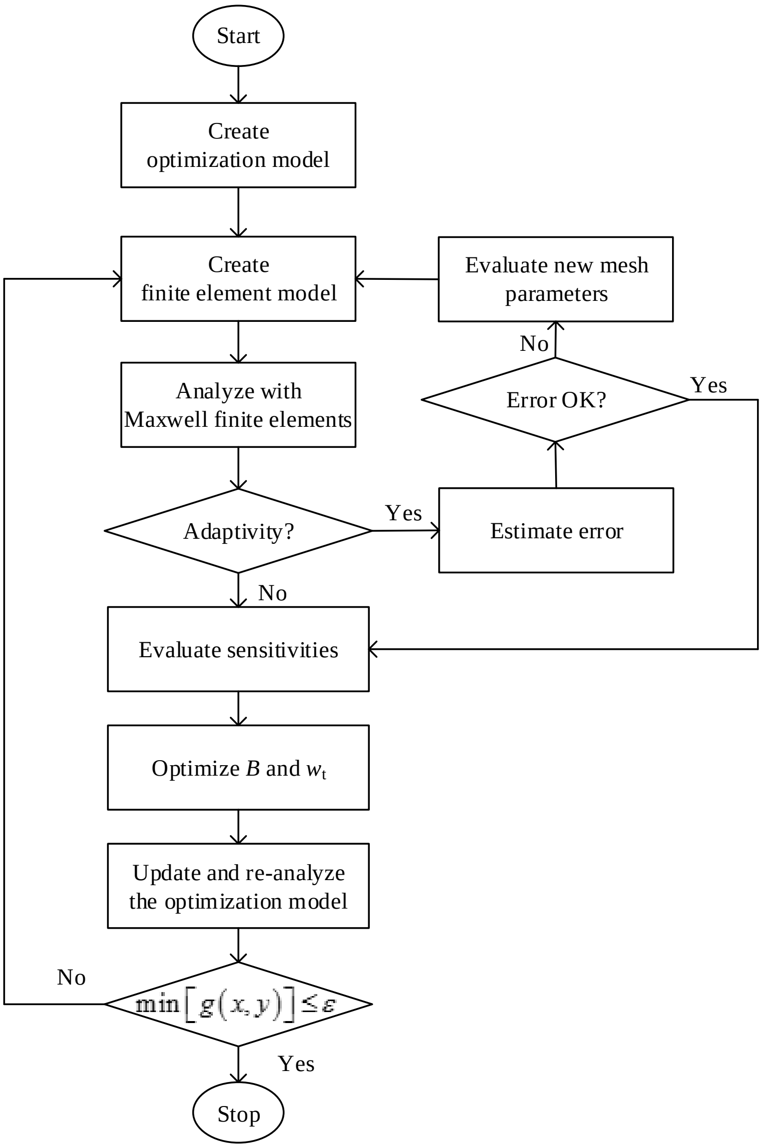

Figure 1. Flowchart of the optimization algorithm with level set evolution.

2.2. The Solution of Level Set Function

Using the discrete grid to represent the level set function, $\phi(x, y, t)$, the distance between adjacent nodes of the discrete grid is h, the time step is Δt, then the level set function at the (i, j) and $n\Delta t$ is:

$$\phi_{ij}^{n} = \phi(ih, jh, n\Delta t) \tag{5}$$

Therefore, the evolution Equation (4) of the level set function, ϕ, can be written as:

$$\frac{\phi_{ij}^{n+1} - \phi_{ij}^{n}}{\Delta t} = F_{ij}^{n}\left|\nabla_{ij}\phi_{ij}^{n}\right| \tag{6}$$

The third-order third-order weighted essentially non-oscillatory (WENO) discrete algorithm is applied to Equation (6) to obtain its solution as:

$$\begin{cases} \phi_{\mathrm{x}} = w_1\phi_{\mathrm{x}}^1 + w_2\phi_{\mathrm{x}}^2 + w_3\phi_{\mathrm{x}}^3 \\ w_1 + w_2 + w_3 = 1 \\ 0 \le w_{\mathrm{i}} \le 1 \end{cases} \tag{7}$$

and

$$\begin{cases} \phi_{\mathrm{x}}^1 = \frac{D\phi_{\mathrm{i}-2}}{3} - \frac{7D\phi_{\mathrm{i}-1}}{6} + \frac{11D\phi_{\mathrm{i}}}{6} \\ \phi_{\mathrm{x}}^2 = -\frac{D\phi_{\mathrm{i}-1}}{3} + \frac{5D\phi_{\mathrm{i}}}{6} + \frac{D\phi_{\mathrm{i}+1}}{3} \\ \phi_{\mathrm{x}}^3 = \frac{D\phi_{\mathrm{i}}}{3} + \frac{5D\phi_{\mathrm{i}+1}}{6} - \frac{D\phi_{\mathrm{i}+2}}{6} \end{cases} \tag{8}$$

where w_{i} is the weight, D is the operator, which is defined as follows:

$$\begin{cases} D_{\mathrm{i}}^0 = \phi_{\mathrm{i}} \\ D_{\mathrm{i}+1/2}^1\phi = \frac{D_{\mathrm{i}+1}^0\phi - D_{\mathrm{i}}^0\phi}{\Delta x} \\ D_{\mathrm{i}}^2\phi = \frac{D_{\mathrm{i}+1/2}^1\phi - D_{\mathrm{i}-1/2}^1\phi}{2\Delta x} \\ \ldots \end{cases} \tag{9}$$

Then, discretize the corresponding time variables, we can get ϕ as:

$$\begin{cases} \frac{\phi^{n+1}-\phi^{n}}{\Delta t} + F_n^n \cdot \nabla\phi^n = 0 \\ \frac{\phi^{n+2}-\phi^{n+1}}{\Delta t} + F_n^{n+1} \cdot \nabla\phi^{n+1} = 0 \\ \phi^{n+1/2} = \frac{3}{4}\phi^{n+1} + \frac{1}{4}\phi^{n+2} \\ \frac{\phi^{n+3/2}-\phi^{n+1/2}}{\Delta t} + F_n^{n+1/2} \cdot \nabla\phi^{n+1} = 0 \\ \phi^{n+1} = \frac{1}{3}\phi^{n} + \frac{2}{3}\phi^{n+3/2} \end{cases} \tag{10}$$

Further, the level set function has the following properties as:

$$\begin{cases} \phi((x,y),t) > 0 \quad \left((x,y) \in \Omega^+\right) \\ \phi((x,y),t) < 0 \quad \left((x,y) \in \Omega^-\right) \\ \phi((x,y),t) = 0 \quad ((x,y) \in \mathrm{C}) \end{cases} \tag{11}$$

Thus, when the level-set method is applied to the shape optimization, the surface formed by ϕ = 0 is used to describe the curve change of C, which can be directly applied to the shape design of electrical machines.

3. CPMLG Optimization with the Level-Set Method

Figure 2 shows the electromagnetic model of the designed CPMLG, including the schematic diagram, winding distribution diagram, and finite element meshing diagram.

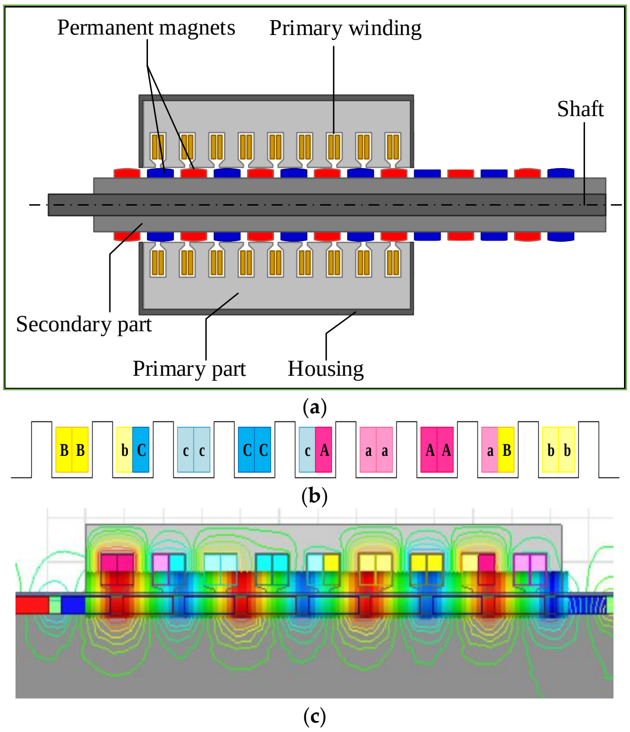

Figure 2. The electromagnetic model of the designed CPMLG. (**a**) Schematic diagram; (**b**) Winding distribution diagram; (**c**) Finite element meshing diagram.

Table 1 presents the main structure parameters of the designed CPMLG.

Table 1. Main structure parameters of the generator.

Structure Parameters	Value	Structure Parameters	Value
Poles p	8	Primary yoke height h_j (cm)	3.3
Pole pitch τ (cm)	8	Primary tooth width b_t (cm)	2.37
Pole-arc coefficient ξ	0.8	Armature effective length l (cm)	158
Primary slots' number	9	Air gap width δ (cm)	0.4
Permanent magnet thickness d (cm)	2	Secondary core thickness d_2 (cm)	16
Width of slot b_s (cm)	4.3	Width of yoke w_t (cm)	2.1

During the simulation procedure, the motion direction is set along the z-axis with the movement displacement being set to 128 cm. The solution step is set to be 0.0005 s. The optimization process is as follows:

(1) The objective air gap magnetic field is given by the mathematical analysis method. Appropriate measuring points are predetermined and the points fully reflect the distribution characteristics of the air gap magnetic field. A contour ring is chosen as the initial shape of the PM with the cross-sectional shape being a 64 mm*10 mm rectangular. So, according to Figure 1 and Equation (11), the corresponding matrix of the zero level-set function is characterized by: The PM boundary value being 0, and the external value and the internal value are equal to 1 and −1, respectively. Then, choose another $n+1$ variables $K_i^{(0)}\left(x_i^{(0)}, y_i^{(0)}\right)$ along the permanent magnet edge evenly to represent the PM shape for optimization. Here, a curvature evolution scheme is

applied under the control lyapunov function (CLF)-condition of the Hamilton-Jacobi equation. Using Equation (10), we can get ϕ and K_i.

(2) Then, the coordinates of K_0, K_1 ... K_n are used to form the profile of the edges of the PMs in ANSYS Maxwell. The magnetic induction density, $B(x_m, y_m)$, at the detection positions, D_0, D_1, ... , D_m, as well as the corresponding x and y axis components of them, $B_x(x_i, y_i)$ and $B_y(x_i, y_i)$, are obtained. According to $B_x(x_i, y_i)$, $B_y(x_i, y_i)$ and their target magnetization values, $B_{x0}(x_i, y_i)$ and $B_{y0}(x_i, y_i)$, we can get the objective function as:

$$g(x,y) = \frac{1}{m}\sum_{i=1}^{m}\left[\frac{\left(B_x(x_i,y_i) - B_{x0}(x_i,y_i)\right)^2 + \left(B_y(x_i,y_i) - B_{y0}(x_i,y_i)\right)^2}{\left(B_{x0}(x_i,y_i)\right)^2 + \left(B_{y0}(x_i,y_i)\right)^2}\right] \tag{12}$$

$$\min[g(x,y)] \leq \varepsilon \tag{13}$$

(3) In addition, $g^{(j)}(x,y)$ is denoted as the jth objective function. In this paper, m = 33. It means that the air gap region corresponding to one pole pair is divided into 32 segments. Figure 3 shows the detection points setting of B.

(4) If the Equation (13) does not hold, then keep F and t unchanged, and repeat the above steps to resolve ϕ and the corresponding $B_x(x_i, y_i)$, $B_y(x_i, y_i)$, and $g(x,y)$ until Equation (13) holds. In this design example, ε and F are set to be 3 and 0.2, respectively. There are five cases of iterations. N is the iteration time and is set to be 100, 200, 300, 400, and 500, respectively. Figure 4 shows the evolution results of the edge of the permanent magnets under five different conditions.

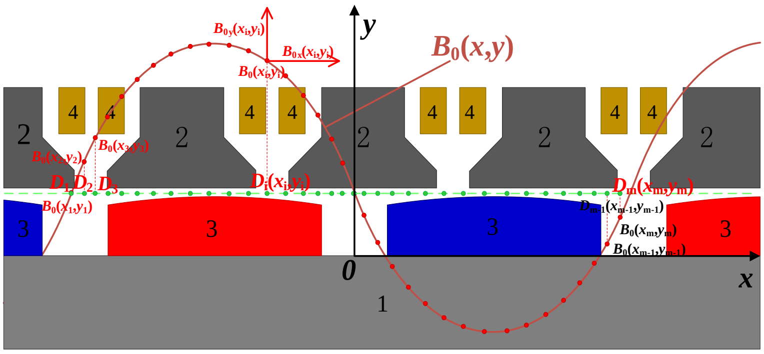

Figure 3. Detection points setting of the B.

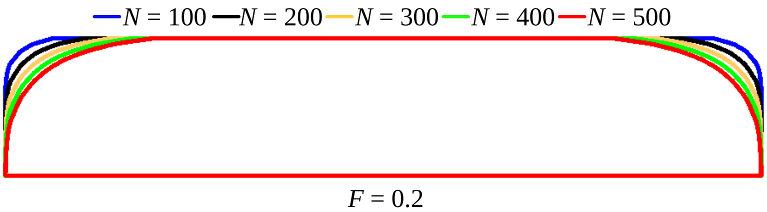

Figure 4. Evolution results of permanent magnets.

4. Simulation Results and Analysis

Figures 5 and 6 shows the flux density and its fast Fourier transform (FFT) decomposition of the designed CPLMG without optimization by the level-set method, respectively, when the wave energy converter drives the generator in constant speed by special techniques [12].

In Figure 6, it shows that the total harmonic distortion (THD) of flux density in the air gap for the CPLMG is about 24.43% before optimization.

The optimization results for CPLMG are shown in Figure 7 and its FFT decomposition with level-set optimization is shown in Figure 8. The related THD of the harmonic content is lower than 24.43%. It is decreased to 17.9%. In addition, there are $g^{(100)}(x,y) = 8.16$, $g^{(200)}(x,y) = 7.47$, $g^{(300)}(x,y) = 4.18$, and $g^{(400)}(x,y) = 2.84$. When $N = 400$, $g^{(400)}(x,y) \leq 3$ satisfies the requirement, so the curve evolution stops. Of course, we can set the ε to be a lower value to get a better performance of the generator.

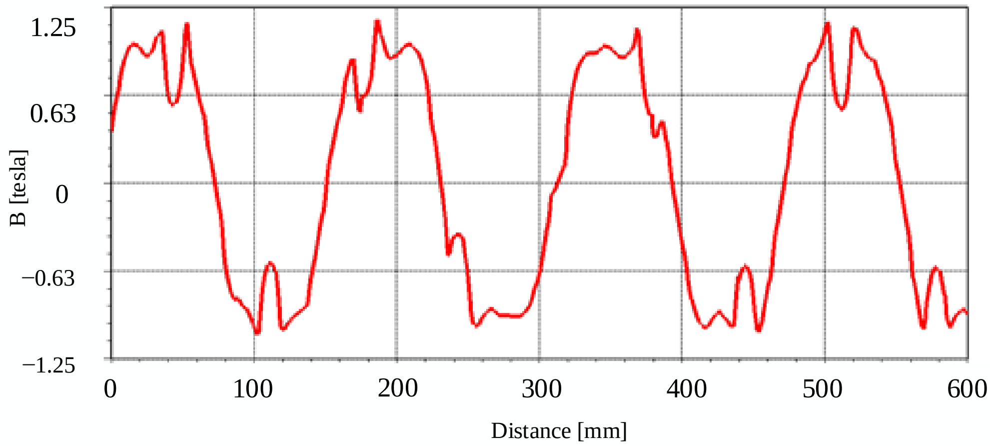

Figure 5. Flux density without optimization.

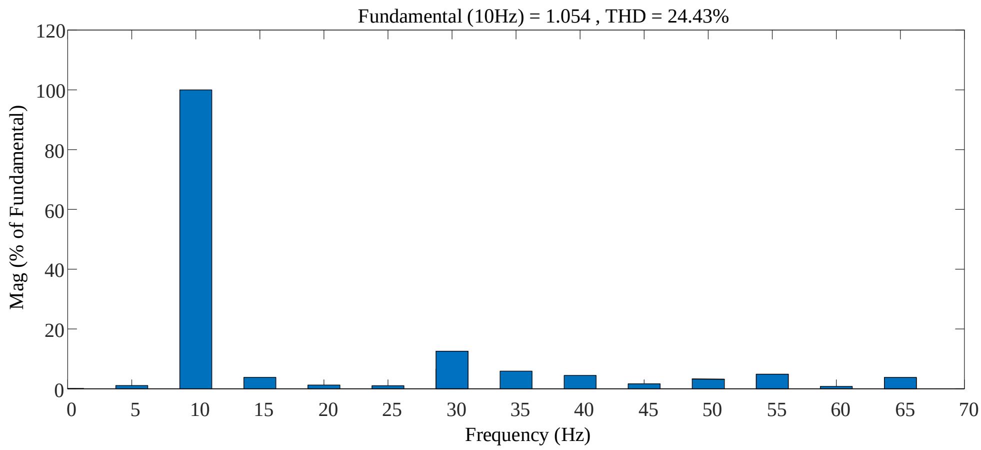

Figure 6. FFT decomposition of flux density without optimization.

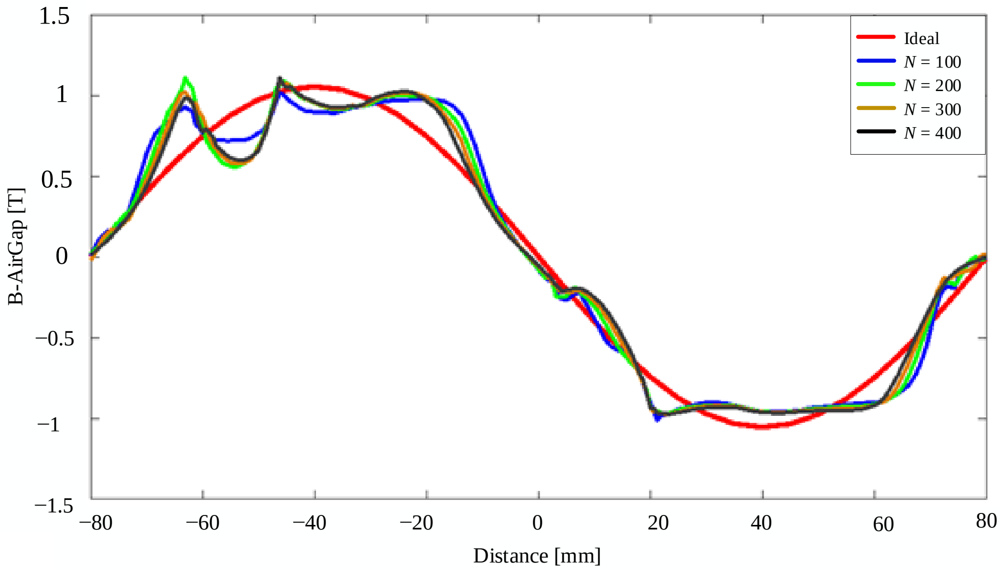

Figure 7. Flux density with level-set optimization.

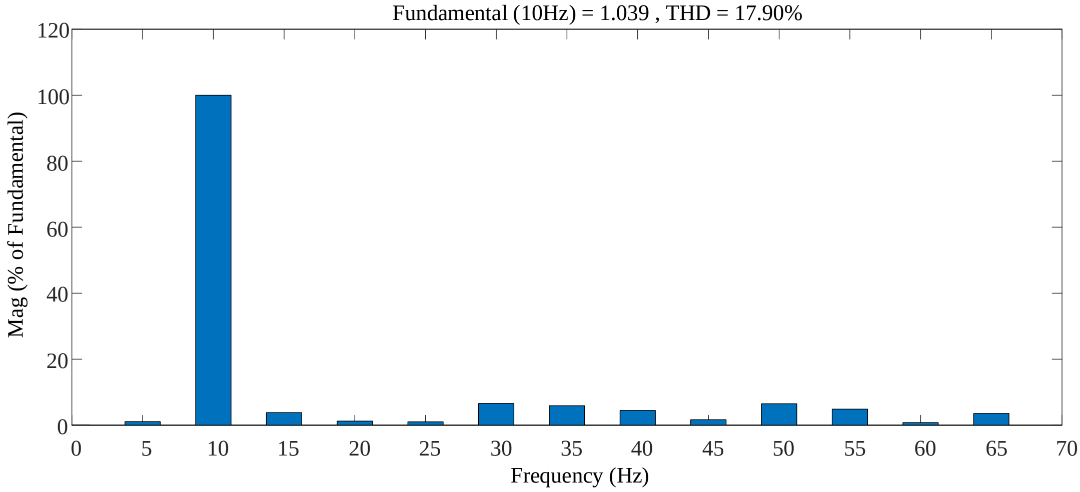

Figure 8. FFT decomposition of flux density with level-set optimization.

Table 2 gives the detection values of B with the level-set optimization at m = 33. Figure 9 presents the optimized permanent magnets model of the generator.

Table 2. Detection values of $B_x(x_i,y_i)$ and $B_y(x_i,y_i)$ with F = 0.2 and N = 400.

i	D_i	$B_x(x_i,y_i)$/T	$B_y(x_i,y_i)$/T
1	D_1	0	0
2	D_2	0.0042	0.1613
3	D_3	0.0061	0.4108
4	D_4	0.0089	0.8153
5	D_5	0.0106	0.8039
6	D_6	0.0276	0.6216
7	D_7	0.0160	0.6447
8	D_8	0.0279	1.0606
9	D_9	0.0626	0.9632
10	D_{10}	0.4018	0.8331
11	D_{11}	0.0529	0.9581
12	D_{12}	0.2064	0.9991
13	D_{13}	0.0417	0.9743
14	D_{14}	0.0101	0.7552
15	D_{15}	0.0062	0.3950
16	D_{16}	0.0034	0.1381
17	D_{17}	−0.0011	−0.0375
18	D_{18}	−0.0799	−0.1977
19	D_{19}	−0.0084	−0.2380
20	D_{20}	−0.0075	−0.4606
21	D_{21}	−0.0074	−0.8741
22	D_{22}	−0.1429	−0.9562
23	D_{23}	−0.2201	−0.9101
24	D_{24}	−0.5251	−0.7700
25	D_{25}	−0.2306	−0.9326
26	D_{26}	−0.3441	−0.9018
27	D_{27}	−0.4879	−0.8190
28	D_{28}	−0.7347	−0.6013
29	D_{29}	−0.0795	−0.9223
30	D_{30}	−0.0100	−0.7101
31	D_{31}	−0.0050	−0.3483
32	D_{32}	−0.0034	−0.0928
33	D_{33}	−0.0006	−0.0074

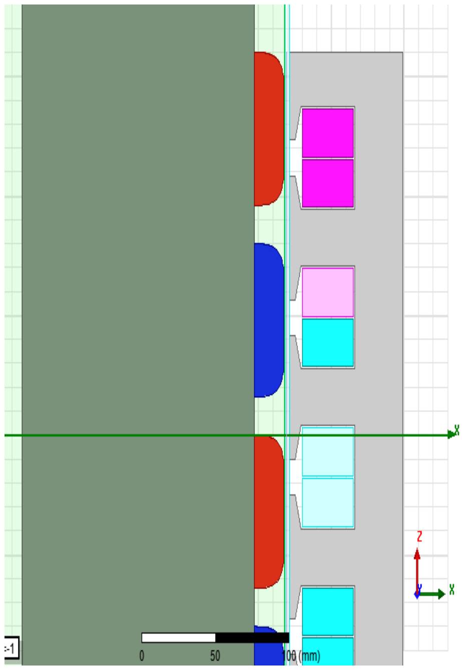

Figure 9. PM model optimized with the level-set method.

Figure 10 shows the three-phase back-EMFs of the CPMLG. In this condition, the width of the yoke is optimized as 1.9 cm so that the unbalance of three-phase back-EMFs is reduced compared with the corresponding results in [23].

Further, the wave energy converter with a mass-adjustable float is used to drive the CPMLG directly [24]. Figure 11 presents the amplitude response curve of the float in the heaving motion direction. Figure 12 shows the related induced voltages with the wave frequency being equal to 0.2 Hz and 0.3 Hz, respectively. From Figure 12, it can be seen that similar maximum peak power and captured energy per period in the steady state are achieved at different wave frequencies.

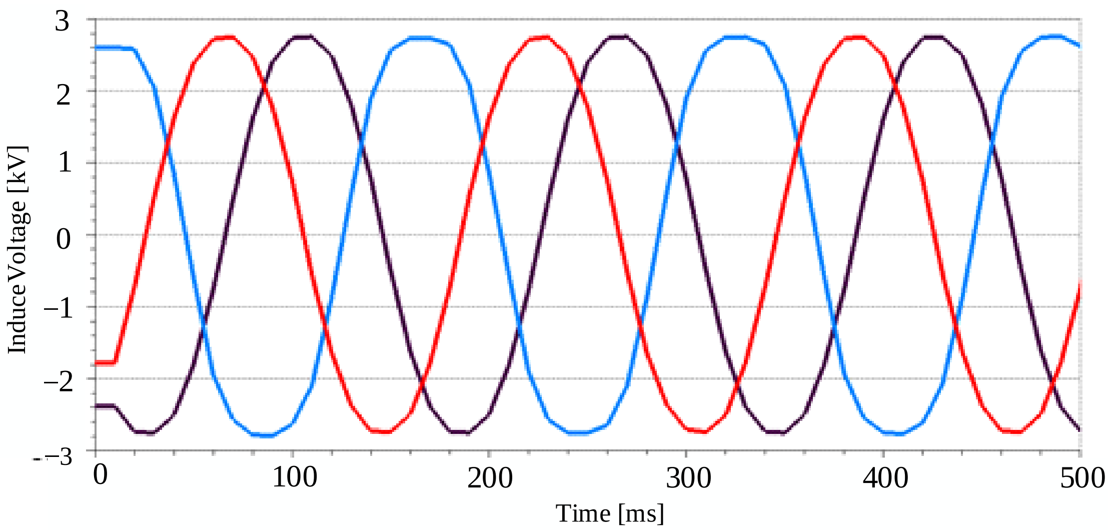

Figure 10. Back-EMF waveform of the CPMLG.

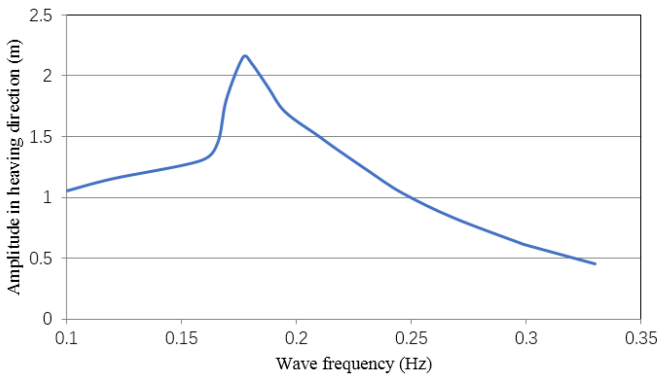

Figure 11. Amplitude of the float motion in the heaving direction.

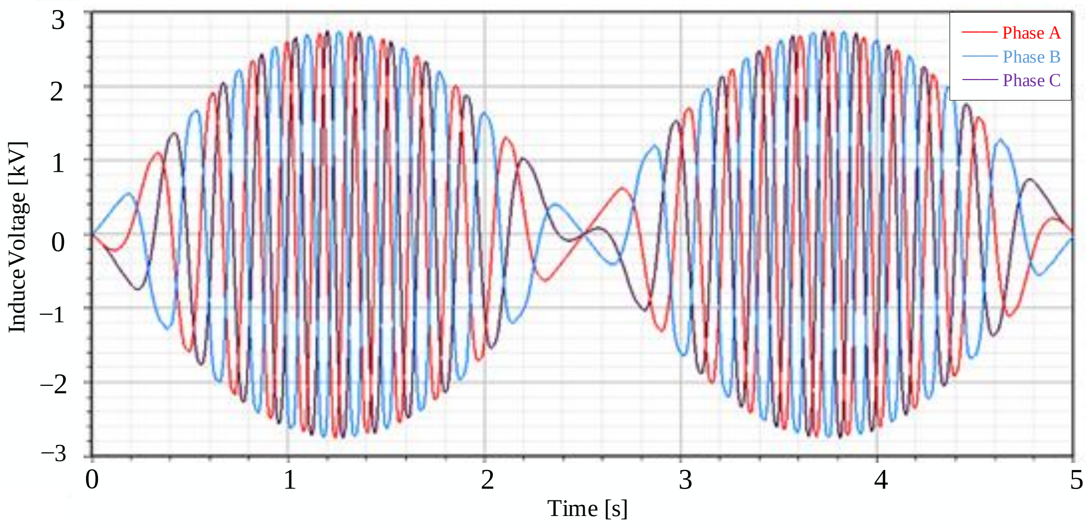

(**a**)

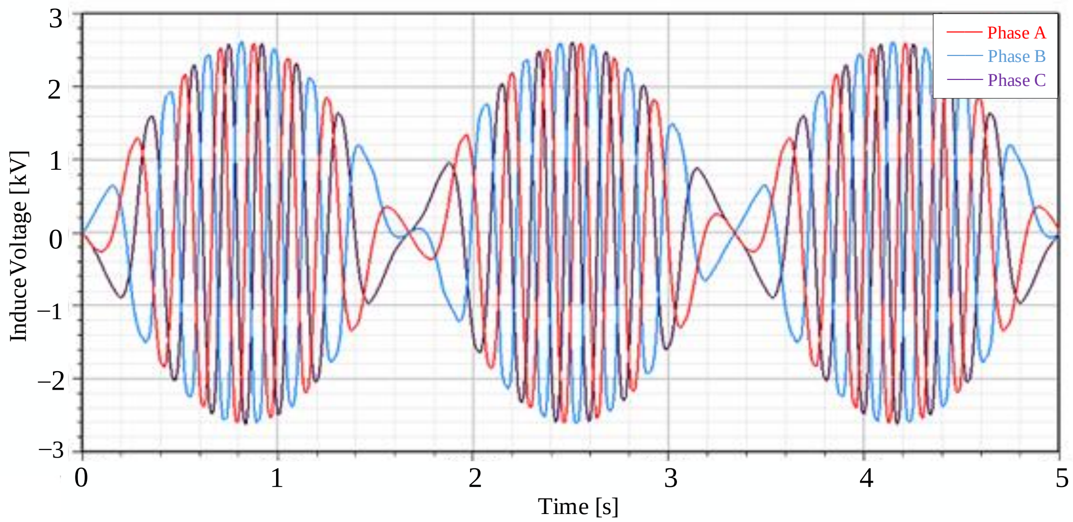

(**b**)

Figure 12. Induced voltages of CPMLG directly driven by WEC. (**a**) 0.2Hz; (**b**) 0.3Hz.

5. Discussions

The results show that the level-set method applied to the topology and size design of the generator is highly reliable in terms of the improvement of the magnetic field distortion. In the electromagnetic model of the designed CPMLG, the unbalance of three-phase back-EMFs and the distortion of air-gap flux density will affect the efficiency and stability of the CPMLG. After setting the optimal air-gap magnetic field and selecting the appropriate detection point, topological evolution of the permanent magnet shape and yoke size are conducted based on the level set equation.

In the paper, the optimization results for CPMLG are compared and discussed. Results show that the related THD of the flux density is decreased after evolution. When the number of iterations reaches 400, it satisfies the optimal condition, and the curve evolution stops. Taking all of these into consideration, it has been proven that the optimal CPMLG electromagnetic model with the set-level method is successful, reliable, and widely applicable.

6. Conclusions

In the paper, to improve the efficiency and reliability of the CPMLG used in a wave energy conversion system, the level set curve evolution method was applied to the design process of the topology evolution of the PM and yoke. The process of topological evolution was analyzed and discussed in detail.

The objective air gap magnetic field was set and an appropriate detection point was given. Based on the specific size of the linear generator, the ideal magnetic waveform was given by the mathematical analysis method. At the same time, air gap magnetic field detection points were selected in the appropriate place in the air gap region. The points fully reflect the distribution characteristics of the air gap magnetic field. Then, topological evolution of the permanent magnet shape was made based on the level set equation. The algorithm was programmed and computed iteratively. Additionally, the shape evolution computation for the PM and yoke could be obtained by using the discrete time and space variables.

Finite element analysis of CPMLG was carried out to obtain the distribution of the air-gap magnetic field and the optimum yoke. The results show that the designed CPMLG can reduce harmonics of the flux density and the unbalance of three-phase back-EMFs. Thus, the adaptability of the generator in wave energy conversion was improved. It has been found that the designed CPMLG can be used for WEC at different wave conditions.

Author Contributions: H.F. designed level set method and wrote the original manuscript; R.S. performed the numerical simulation and analyzed the numerical results; Z.X. visualized the results, revised the manuscript and polished the English.

Acknowledgments: The work was supported by a grant from National Natural Science Foundation of China (No. 51577124, No.51877148).

Conflicts of Interest: The authors declare no conflict of interest.

References

1. Balitsky, P.; Verao Fernandez, G.; Stratigaki, V.; Troch, P. Assessment of the Power Output of a Two-Array Clustered WEC Farm Using a BEM Solver Coupling and a Wave-Propagation Model. *Energies* **2018**, *11*, 2907. [CrossRef]
2. Wu, J.; Yao, Y.; Zhou, L.; Göteman, M. Latching and Declutching Control of the Solo Duck Wave-Energy Converter with Different Load Types. *Energies* **2017**, *10*, 2070. [CrossRef]
3. Guardeño, R.; Consegliere, A.; López, M.J. A Study about Performance and Robustness of Model Predictive Controllers in a WEC System. *Energies* **2018**, *11*, 2857. [CrossRef]
4. Franzitta, V.; Curto, D.; Milone, D.; Rao, D. Assessment of Renewable Sources for the Energy Consumption in Malta in the Mediterranean Sea. *Energies* **2016**, *9*, 1034. [CrossRef]
5. Jones, C.; Chang, G.; Raghukumar, K.; McWilliams, S.; Dallman, A.; Roberts, J. Spatial Environmental Assessment Tool (SEAT): A Modeling Tool to Evaluate Potential Environmental Risks Associated with Wave Energy Converter Deployments. *Energies* **2018**, *11*, 2036. [CrossRef]
6. Feng, N.; Yu, H.; Hu, M.; Liu, C.; Huang, L.; Shi, Z. A Study on a Linear Magnetic-Geared Interior Permanent Magnet Generator for Direct-Drive Wave Energy Conversion. *Energies* **2016**, *9*, 487. [CrossRef]

7. Huang, L.; Hu, M.; Chen, Z.; Yu, H.; Liu, C. Research on a Direct-Drive Wave Energy Converter Using an Outer-PM Linear Tubular Generator. *IEEE Trans. Magn.* **2017**, *53*, 8104704. [CrossRef]
8. Xia, T.; Yu, H.; Chen, Z.; Huang, L.; Liu, X.; Hu, M. Design and Analysis of a Field-Modulated Tubular Linear Permanent Magnet Generator for Direct-Drive Wave Energy Conversion. *IEEE Trans. Magn.* **2017**, *53*, 8103904. [CrossRef]
9. Zhang, J.; Yu, H.; Shi, Z. Design and Experiment Analysis of a Direct-Drive Wave Energy Converter with a Linear Generator. *Energies* **2018**, *11*, 735. [CrossRef]
10. Zhang, C.; Chen, F.; Li, L.; Xu, Z.; Liu, L.; Yang, G.; Lian, H.; Tian, Y. A Free-Piston Linear Generator Control Strategy for Improving Output Power. *Energies* **2018**, *11*, 135. [CrossRef]
11. Prudell, J.; Stoddard, M.; Amon, E.; Brekken, T.K.A.; von Jouanne, A. A Permanent-magnet Tubular Linear Generator for Ocean Wave Energy Conversion. *IEEE Trans. Ind. Appl.* **2010**, *46*, 2392–2400. [CrossRef]
12. Fang, H.W.; Wang, D. Design of Permanent Magnet Synchronous Generators for Wave Power Generation. *Trans. Tianjin Univ.* **2016**, *22*, 396–402. [CrossRef]
13. Farrok, O.; Islam, M.R.; Sheikh, M.R.I.; Guo, Y.G.; Zhu, J.G.; Xu, W. A Novel Superconducting Magnet Excited Linear Generator for Wave Energy Conversion System. *IEEE Trans. Appl. Superconduct.* **2016**, *26*, 5207105. [CrossRef]
14. Zhu, Z.Q.; Hu, J. Electrical Machines and Power Electronic Systems for High-Power Wind Energy Generation Applications: Part II- Power Electronics and Control Systems. *Int. J. Comput. Math. Electr. Electr. Eng.* **2013**, *32*, 7–33. [CrossRef]
15. Liu, C.Y.; Yu, H.T.; Hu, M.Q.; Liu, Q.; Zhou, S.G.; Huang, L. Research on a Permanent Magnet Tubular Linear Generator for Direct Drive Wave Energy Conversion. *IET Renew. Power Gener.* **2014**, *8*, 281–288. [CrossRef]
16. Tom, N.; Yeung, R.W. Experimental Confirmation of Nonlinear-Model-Predictive Control Applied Offline to a Permanent Magnet Linear Generator for Ocean-Wave Energy Conversion. *IEEE J. Ocean. Eng.* **2016**, *41*, 281–295.
17. Sethian, J.A. *Variational Methods for Tree Surface Interfaces*; Numerical Methods for Propagating: New York, NY, USA, 1987; pp. 155–164.
18. Osher, S.J.; Sethian, J.A. Fronts Propagating with Curvature Dependent Speed: Algorithms Based on Hamilton-Jacobi Formulation. *J. Comput. Phys.* **1988**, *79*, 12–49. [CrossRef]
19. Ruiz-España, S.; Díaz-Parra, A.; Arana, E.; Moratal, D. A Fully Automated Level-Set Based Segmentation Method of Thoracic and Lumbar Vertebral Bodies in Computed Tomography images. In Proceedings of the 2015 37th Annual International Conference of the IEEE Engineering in Medicine and Biology Society (EMBC), Milan, Italy, 25–29 August 2015; pp. 3049–3052.
20. Kim, Y.S.; Park, I.H. Topology Optimization of Rotor in Synchronous Reluctance Motor Using Level Set Method and Shape Design Sensitivity. *IEEE Trans. Appl. Supercond.* **2010**, *20*, 1093–1096.
21. Putek, P.; Paplicki, P.; Pałka, R. Low Cogging Torque Design of Ppermanent Magnet Machine Using Modified Multi-Level Set Method with Total Variation Regularization. *IEEE Trans. Magn.* **2014**, *50*, 657–660. [CrossRef]
22. Kwack, J.; Min, S.; Hong, J.P. Optimal Stator Design of Interior Permanent Magnet Motor to Reduce Torque Ripple Using the Level Set Method. *IEEE Trans. Magn.* **2010**, *46*, 2108–2111. [CrossRef]
23. Fang, H.W.; Chen, H.X. Design of Cylindrical Permanent Magnet Linear Generator for Ocean Wave Energy Conversion with Level-Set Method. In Proceedings of the Compumag: Conference of Electromagnetic Fields (Compumag 2017), Seoul, Korea, 18–22 June 2017.
24. Fang, H.W.; Jin, L.T. A Wave Frequency Adaptive Wave Energy Conversion System. Chinese Patent 201810070154, 6 January 2018.